

See discussions, stats, and author profiles for this publication at: <https://www.researchgate.net/publication/332978644>

# Superbat: Battery like supercapacitor utilized by graphene foam and zinc oxide (ZnO) electrodes induced by structural defects

Article · May 2019

DOI: 10.1039/C9NA00199A

CITATIONS

5

READS

146

4 authors:



**Sibel Kasap**

Sabanci University

29 PUBLICATIONS 108 CITATIONS

[SEE PROFILE](#)



**Ismet Inonu Kaya**

Sabanci University

54 PUBLICATIONS 349 CITATIONS

[SEE PROFILE](#)



**Sergej Repp**

University of Freiburg

19 PUBLICATIONS 502 CITATIONS

[SEE PROFILE](#)



**Emre Erdem**

Sabanci University

98 PUBLICATIONS 2,075 CITATIONS

[SEE PROFILE](#)

Some of the authors of this publication are also working on these related projects:



eBook "Frontiers in Magnetic Resonance: Electron paramagnetic resonance in modern carbon-based nanomaterials" [View project](#)



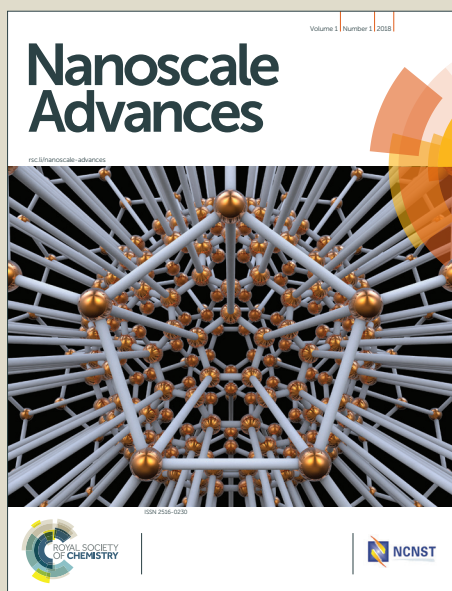
Investigation of adsorption capacity of 3D-graphene foam for radionuclides [View project](#)

# Nanoscale Advances

Accepted Manuscript



This article can be cited before page numbers have been issued, to do this please use: S. Kasap, I. I. Kaya, S. Repp and E. Erdem, *Nanoscale Adv.*, 2019, DOI: 10.1039/C9NA00199A.



This is an *Accepted Manuscript*, which has been through the Royal Society of Chemistry peer review process and has been accepted for publication.

*Accepted Manuscripts* are published online shortly after acceptance, before technical editing, formatting and proof reading. Using this free service, authors can make their results available to the community, in citable form, before we publish the edited article. We will replace this *Accepted Manuscript* with the edited and formatted *Advance Article* as soon as it is available.

You can find more information about *Accepted Manuscripts* in the [Information for Authors](#).

Please note that technical editing may introduce minor changes to the text and/or graphics, which may alter content. The journal's standard [Terms & Conditions](#) and the [Ethical guidelines](#) still apply. In no event shall the Royal Society of Chemistry be held responsible for any errors or omissions in this *Accepted Manuscript* or any consequences arising from the use of any information it contains.

# Superbat: Battery like supercapacitor utilized by graphene foam and zinc oxide (ZnO) electrodes induced by structural defects

View Article Online  
DOI: 10.1039/C9NA00199A

Sibel Kasap<sup>1</sup>, Ismet I. Kaya<sup>1,2</sup>, Sergej Repp<sup>3</sup>, Emre Erdem<sup>1, 2,\*</sup>

<sup>1</sup>Sabanci University, SUNUM Nanotechnology Research Centre TR-34956 Istanbul, Turkey

<sup>2</sup>Faculty of Engineering and Natural Sciences, Sabanci University, TR-34956, Istanbul, Turkey

<sup>3</sup>University of Freiburg, Institute of Physical Chemistry, Albertstr. 21, 79104 Freiburg, Germany

\*email: emreerdem@sabanciuniv.edu

## Abstract

The current work presents a hybrid type of energy storage device composed of both graphene foam and zinc oxide electrodes which exhibit both electrochemical performances of supercapacitor with relatively higher powder density and battery with relatively higher energy density as compared to each individual component as single devices. And, they correlate the hybrid performance to the defective structure of the electrodes. To enhance the electrochemical performance of supercapacitors it is necessary to have well-defined mass, shape and surface area of electrode materials. Here we present original design mounting device that enable to determine precisely the all critical parameters of electrode materials in particular mass and surface area. By the aid of the original setup we produced supercapacitor device which act as battery due to its high energy density values, hence we named it as *superbat*. In this work, 3D graphene foam was used as first electrode due to its large surface. As second electrode ZnO nanocrystals were used as second electrode for its defective structure. Paramagnetic resonance Raman and impedance spectroscopy have been undertaken in order to understand the origin of the performance of hybrid capacitor in more depth. In particular, we obtained high specific capacitance value ( $C = 448 \text{ F/g}$ ) which is exceptionally related not only the quality of synthesis but also the choice of electrode and electrolyte materials. Moreover, each component used in the construction of the hybrid supercapacitor is also played a key role to achieve high capacitance value. The results demonstrated the remarkable performance and stability of the *superbat*.

## 1. Introduction

Exploring properties of materials for battery and supercapacitor applications is one of the “dirtiest” kind research not only because of its hazardous basic components such as electrodes, electrolytes and their solvents, separators and current collectors but also thousands of publications in the literature which present enormous number of electrochemical performance results. Electrode materials are often used in supercapacitors or batteries with little or no investigation on their defect structures which in fact play a crucial role in their electronic, magnetic, optical and mechanical behavior thus, in this context, their electrochemical performance. Electrodes are key components for the production of supercapacitors and the strategies for selecting the electrodes play a decisive role



in their specific power and energy storage performance. For instance, one strategy is to decrease the crystal size to nanometer scale in order to increase the surface area and have more active sites and shorter ionic paths. Another strategy is to use composite materials to achieve higher conductivity and more structural stability. Such critical decisions in the selection of electrode materials make supercapacitor applications highly diverse and open to new developments. Today, batteries and supercapacitors are introduced as the principal energy storage media for so called “clean-energy” or “green-energy” in electrically driven devices such as electric vehicles. Lithium, some transition metal ions such as Co, Mn, Fe, and carbonaceous materials including graphite, graphene oxide and carbon black are the most common electrode materials in batteries, whereas lithium hexafluorophosphate (LiPF<sub>6</sub>) is the most common electrolyte salt. Therefore, while speaking about “clean-energy” in electricity production and storage, hazards of such materials also need to be taken into serious consideration. Such environmental issues which may play a role in energy policies are not the main focus of this work but the defect structures are.

Thanks to the tremendous progress in the research and technology in the field, supercapacitor based electrical energy storage devices are recently becoming one-step closer to being alternative to the traditional Li-ion batteries due to enhancement in their energy storage capacity<sup>1–3</sup>. Indeed, the supercapacitor technology can reach to a milestone, where the energy storage systems can both have high energy capacity and deliver high output power by combining multifunctional materials with smart designs. On the other hand, our recent investigations on supercapacitors<sup>4,5</sup> motivated us to tackle some challenges that still need to be addressed for building better supercapacitors. There are different types of supercapacitors in terms of their operating mode principles and designs, namely electrostatic double-layer capacitors (EDLCs), electrochemical pseudocapacitors and hybrid capacitors. It is well known that pseudocapacitors are capable to store much more electrical energy compared to standard supercapacitors. In this work, electrochemical pseudocapacitors will be used with a distinct efficient design where the supercapacitor may act as a battery. Such a system can be called as “*superbat*” and may have potential applications in future electric vehicles, wearable electronics, nanogenerators and microelectronic devices. In fact, *superbat* construction is similar to that of batteries but the principle of operation is different. In a *superbat*, there are two electrodes, a separator, and an electrolyte containing negative and positive ions, as in a battery. In the charging state negative and positive ions move towards the electrodes and they are absorbed on their surface. Such reactions occur very fast and hence enable a *superbat* to deliver high-power. To reach the ultimate goal of high energy storage, rated potential of a *superbat* needs to be improved simply because of the fundamental energy density relation:  $E = \frac{1}{2}C(\Delta V)^2 \times (1/3.6)$ , where  $E$  is the stored energy (Wh/kg),  $\Delta V$  is the operating voltage (V) and  $C$  is the specific capacitance (F/g). Consequently, the maximum power density of *superbat*  $P_{\max}$  which can be determined from the low frequency result of impedance via relation:  $P_{\max} = V_{\max}^2/4m_tR_{\text{ESR}}$  where  $V_{\max}$  is the maximum charging voltage,  $R_{\text{ESR}}$  is the equivalent series resistance and  $m_t$  is the total mass of the both electrodes.  $P$  and  $E$  relate with each other by time as follows:  $P = 3600(E/\Delta t)$  where  $\Delta t$  is the discharge time. Obviously, in this perspective one has to ensure the stability of the electrolyte which can be degraded beyond a critical potential, decomposed into a gas state and become unstable (i.e., 4.2 V for LiPF<sub>6</sub>). To understand the electrochemical performance of the *superbat* systems, we first study the defect structures of the electrode materials that were used in this work, namely graphene foam (GF) and ZnO nanocrystals by electron paramagnetic resonance (EPR) spectroscopy. EPR is well suited for understanding the role of structural defect centers since it provides a direct method to monitor different paramagnetic states of defects. Therefore, it complements other analytical experimental techniques such as Raman



spectroscopy. Moreover, due to insufficient analytical characterization of the electrode materials and the lack of data from advanced EPR techniques, which preclude the unambiguous determination of defect states, the role of structural point defects on electrochemical performance remain unclear and is still a matter of debate. This is mainly due to the fact that, at present most of the researchers who investigate supercapacitors or batteries are trying to improve energy or power density, charge/discharge time and cycling stability while overlooking the effect of defect structures at microscopic scale. For instance, one of the rare defect studies unambiguously demonstrated that structural defects in the crystals of  $\text{NaCrO}_2$  electrodes played a significant role in achieving high specific capacity and excellent capacity retention for sodium ion batteries <sup>6</sup>. In another study which is about the critical role of point defects in  $\delta\text{-MnO}_2$  nanosheets, it has been shown that Mn vacancies provide ion intercalation sites which simultaneously enhance specific capacitance, charge transfer resistance and cycling stability <sup>7</sup>. Nowadays, due to their high specific capacitance and low resistance, metal oxides such as  $\text{ZnO}$ ,  $\text{In}_2\text{O}_3$ ,  $\text{MnO}_2$ ,  $\text{RuO}_2$  etc. have great potential in designing of superbats with high energy and power density <sup>8,9</sup>. Very recently, it has been reported that  $\text{ZnO}$  based composite electrode materials can provide good electrochemical reversibility, high specific capacitance, high power density, high energy density and good cycling stability, which makes them promising materials for advanced supercapacitors <sup>10</sup>. In particular,  $\text{ZnO}$  is a highly defective wide band-gap semiconductor and a luminescent material in which defect centers play a vital role in its ionic and electronic transport properties. Conceivably, some of the possible intrinsic defect centers in  $\text{ZnO}$  are: (i) zinc vacancies, (ii) zinc on interstitial sites, (iii) oxygen on interstitial sites, and (iv) oxygen vacancies. EPR active intrinsic defect centers have previously been discussed in detail elsewhere <sup>11–14</sup>. Within the framework of our recent EPR studies on  $\text{ZnO}$  nanoparticles, two distinct EPR spectral features have been identified as defect centers that are located at the core and on the surface with  $g$ -factors 1.962 and 2.004, respectively <sup>14–16</sup>. The difficult task of understanding the origin of intrinsic defects and their assignment, both at the bulk and the surface of  $\text{ZnO}$  nanocrystals that are synthesized via various routes are partly solved by semi-empirical core-shell model. EPR and photoluminescence spectroscopic investigations have been instrumental in explaining the origin of different defect types in nanosized  $\text{ZnO}$ , and the temperature dependence and microwave saturation behavior of localized and delocalized electrons by that model <sup>11,12,17</sup>. On the other hand, carbonaceous materials are also highly defective; such as dangling bonds and C-radicals can be detected via EPR technique <sup>18,19</sup>. Recent EPR studies delivered detailed information on the defect structure of carbonaceous materials not only providing insight into their spin properties, which includes conduction electrons, unpaired spins and dangling bonds, but also enabling investigation of electronic states in different forms of carbon. Even  $\text{ZnO}$  decorated with hybrid graphene materials has revealed interesting EPR results indicating competing and healing effects of the intrinsic defects involved both in  $\text{ZnO}$  and graphene <sup>19</sup>.

Graphene based composites, in particular, have recently been attracting high attention, due to their potential application in energy storage devices such as batteries and supercapacitors <sup>1,20</sup>. Graphene possesses a single atomic layer where  $sp^2$  hybridized carbon atoms are arranged in a honeycomb-like a two-dimensional (2D) network. Such an exclusive structural peculiarity results in a tunable large specific surface area, high thermal conductivity as well as a very high intrinsic mobility of charge carriers <sup>21</sup>. However, 2D graphene sheets have strong tendency to aggregate and to restack in macroscopic scale because of the strong  $\pi$ - $\pi$  interactions between individual sheets. This tendency leads to reduction in effective surface area and limit the surface available for electrochemical double layer formation. Therefore, the usage of 2D graphene sheets in electrochemical applications is



limited<sup>22,23</sup>. To overcome these drawbacks, three dimensional (3D) macroscopic graphene structures including sponge, foam, hydrogel and aerogel have been developed, recently<sup>24</sup>. These macroscopic structures not only retain most of the precious properties of 2D graphene such as high electrical conductivity and large specific surface area but also offer low density and good mechanical strength<sup>25–28</sup>. Among them, foam-like 3D graphene structures have attracted attention in electrochemical applications because of their porous and well-defined morphology. GF morphology not only ensures fast electron transfer but also allow combining other electrochemically active materials which enhance the super capacitive performance<sup>22,27</sup>. Utilization of a self-assembly method to prepare graphene oxide (GO) followed by a reduction process using strong chemical oxidants is the most common method to produce foam-like macroscopic structures. Although massive amount of 3D-GF can be produced by this technique, foam structures contain defects and exhibit low electrical conductivity<sup>29,29–31</sup>. In contrary to self-assembly method, chemical vapor deposition (CVD) method to produce 3D graphene foams with more controlled and uniform morphologies and structures with large area. Via this process flow, free-standing graphene foams with high electrical conductivity and improved structural stability superior to the chemically derived graphene sheets can be produced<sup>32,33</sup>. From the electrochemical performance point of view, several graphene-decorated models have already been introduced to enhance the capacitance for energy storage applications. Such models illustrated significant improvement in capacitance that are attributed to extra and deeper redox reactions, which are due to the enhancement of conductivity via defect structures and dispersion due to the incorporation of graphene<sup>34,35</sup>. Therefore, in any energy storage device such as a battery or a capacitor, the role of defect structures in the electrode materials needs to be thoroughly investigated. Recently the importance of vacancies in functional materials for clean energy storage and harvesting were reported as “the perfect imperfection” pointing out that by the extensive controlling of defect centers one may influence the materials physical and chemical properties such as band gap and conductivity thus the electrochemical performance of electrode materials<sup>36</sup>.

Basics of the above-mentioned properties and applications of carbonaceous materials have already been presented in excellent comprehensive and focused reviews or monographs in the framework of supercapacitor technology<sup>9,37–40</sup>.

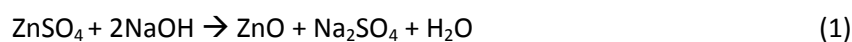
However, there have been only a few EPR studies performed on graphene and graphene-like structures such as 3D-GF. For example, two distinct EPR spectra of reduced graphene oxide (rGO) were reported: a broad spectrum at  $g = 2.0027$ , which can be attributed to graphite-like carbon and a narrower spectrum at  $g = 2.0028$  associated with carbon radicals. Since graphene is also phonon-mediated active carbon, the electron-phonon interaction plays an important role in the hybridization mechanism which is essentially responsible for large surface area. However, unclear issues such as the Kohn anomaly, the broadening/shift in D- and G- bands, the anharmonicity, and multi-phonon contributions may be closely related with the defects. The importance of phonon-defect interaction as an alternative cause for the anomalies of graphene has been reported in former reports. Therefore, the correlation of Raman and EPR spectroscopy results would give conceivable information about the defect related electron-phonon or phonon-defect interactions, which most likely effect the electrochemical performance of energy storage and power devices hence, *superbats*. Both of these versatile experimental methods complement each other in exploring fundamental properties of graphene and ZnO and characterizing the type of defects, defect-phonon interactions and electrical transport<sup>5,41,42</sup>.



In the present study, basically, the hybrid superbat has been assembled by the aid of four main components: Graphene foam and ZnO nanocrystals as next generation electrodes, 1 M LiPF<sub>6</sub> in ethylene carbonate and ethyl methyl carbonate (EC/MC=50/50) as electrolyte and glass fiber (GF) as separator. Overall, the reason why we used these materials and our main strategy to increase the device performance can be described as follows: Unlike EDLCs, pseudocapacitors store energy through Faradic reactions, comprising fast and reversible redox reactions between electrode materials and electrolyte on the electrode surface. Usually, pseudocapacitors which contain metal oxides reveal higher capacitance than those of EDLCs due to their different charge storage mechanism. However, they often suffer from stability problems due to low electrical conductivity. Hybrid superbat is a smart arrangement of EDLCs and pseudocapacitors, in which EDLCs and Faradic capacitance may contribute to overall performance instantaneously. Moreover, the existence of defect structures in ZnO and GF and their synergetic effects on the hybrid *superbat* could improve the overall conductivity of the system, thus the electrochemical stability and the performance. This is quite reasonable while the high conductivity can contribute to the reduction of internal resistance resulting in a high power density. However on one side it is well known that defects can improve the conductivity of ZnO and on other side as the defects increase in a metal / semi-metal such as a graphene, the conductivity is expected to decrease. So it is quite challenging issue to understand the mechanism of how such intrinsic defects in a complete supercapacitor device. It is clear that competing effects will occur and such effects will mainly affect the performance of the device. Thus it is quite difficult to say how the defects of GF and ZnO influence individually the performance of the *superbat*. Nevertheless, equipped with such supreme properties, *superbats* start to emerge as an efficient energy storage technology that may take an essential role in energy systems in the future.

## 2. Experimental

**A. Synthesis of ZnO nanocrystals:** In order to understand the effect of defects we have used a specific method to synthesize defective ZnO nanocrystals. Solid state (SS) synthesis method enables us not only to characterize the defect centers under different conditions but also provides a good control on the mean size, size distribution, and morphology of the nanocrystals. Detailed description and characterization of the SS synthesized ZnO nanocrystals can be found elsewhere<sup>13</sup>. Briefly, in this method we have used the following chemicals with the highest purity available: Zinc sulfate (ZnSO<sub>4</sub>, Aldrich, purity 99%), sodium hydroxide (NaOH, Roth, purity 99%). We grounded NaOH and ZnSO<sub>4</sub> with the molar ratio of 2:1 respectively in a mortar for 30 minutes at room temperature (RT). After that, we washed the solid mud by adding millipore water and then washed the suspension several times. Finally, the powder was dried for 2 hours at 80 °C in an oven. We obtained ZnO nanocrystals by calcinating this precursor at different calcination temperatures (CT) ranging from 300 °C up to 600 °C. The calcination process was done as follows: 23°C (RT) (heating rate 8.3 °C/min) → CT (2 h) → free cooling to RT. The product was grounded by pestle and mortar. The chemical equation in SS reaction is as follows:



**B. Synthesis of graphene foam:** The 3D GF macrostructure was synthesized on a nickel foam with 16 mm thickness ( $\geq 95\%$  porosity, 99.99% purity) via chemical vapor deposition (CVD) method. The nickel foam ( $5 \times 5 \text{ cm}^2$ ) was placed horizontally in the central zone of the quartz tube in the CVD chamber and heated up to  $1000 \text{ }^\circ\text{C}$  with a flow of Ar (250 sccm) and  $\text{H}_2$  (100 sccm) gas mixture at low pressure (60 mbar). To remove oxide layer on its surface, the nickel foam was maintained for 10 min under that condition. Then, 100 sccm  $\text{CH}_4$  gas as a carbon precursor was delivered into the quartz tube for 60 min to grow graphene sheets on the nickel template. Following this step, the sample was allowed to cool to ambient temperature naturally under an Ar gas flow. In order to obtain the free-standing graphene macrostructure, the nickel template was etched in 1 M  $\text{FeCl}_3$  solution for 24 h. After the etching, the 3D graphene foam was immersed in a DI-water/HCl mixed solution (1:1 (v/v)) to clean it from iron residues. Finally, the graphene foam was dried at  $80 \text{ }^\circ\text{C}$  for 30 min in an oven.

**C. Design of the *superbat*:** The design sketch and all of the components of the *superbat* can be seen in the illustration in Fig 1(a). The photographs in Fig 1(b) present the prototype home-made capacitor mounting system. The main difference of *superbat* design compare to conventional two-electrode setup, such as commercial T-shape Swagelok two-electrode system, is defined diameter and weight of electrodes and also well control insertion of them into the device. Moreover, stainless steel current collectors are highly effectively designed to measure the current and voltage. This device practically does not require to measure the electrochemical response of both electrodes independently in a three-electrode device to study the reactions taking place while here the main aim is to see directly the synergy of the materials all together.



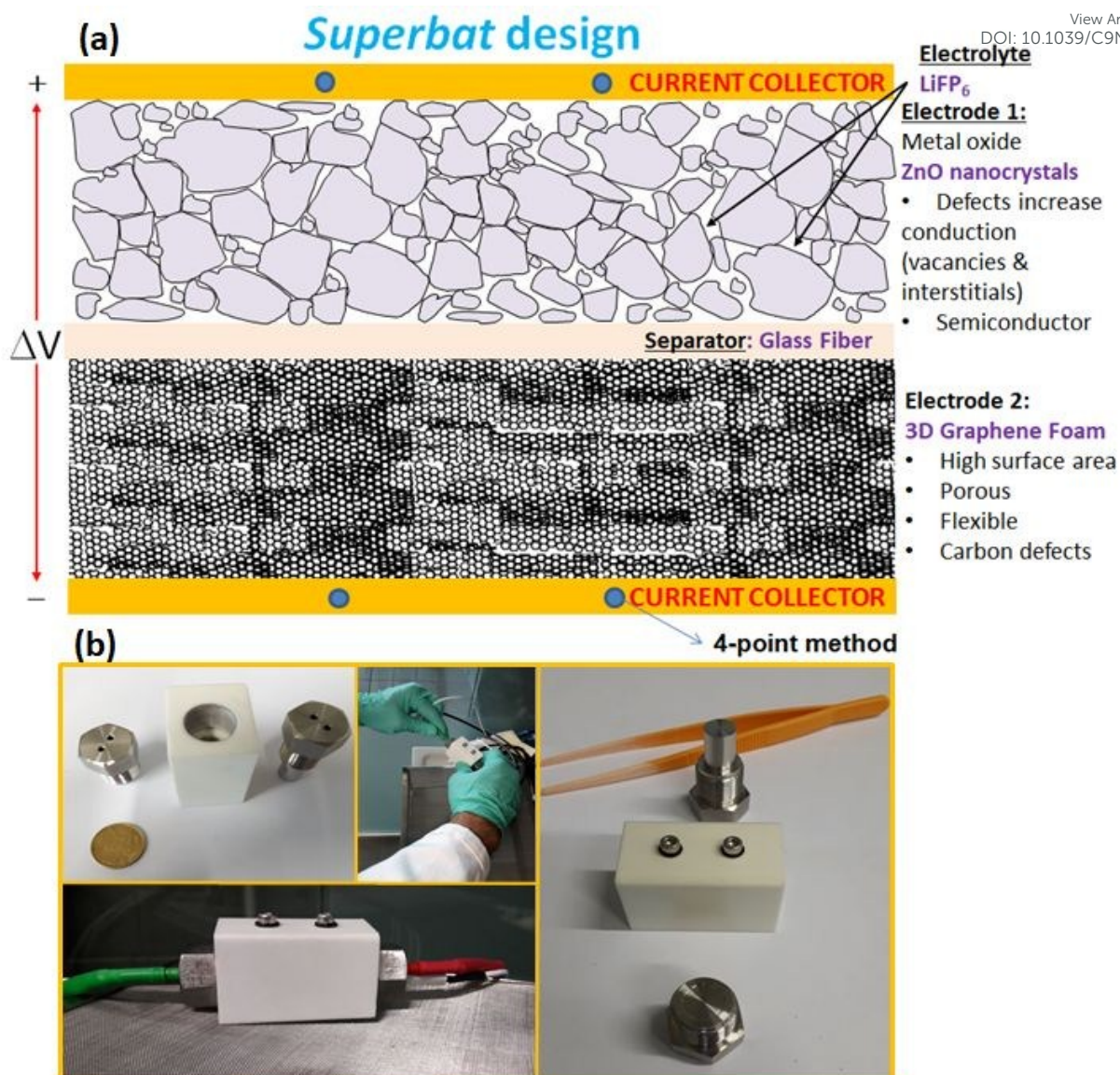


**Fig. 1:** (a) The *superbat* design consisting of four basic components. Advanced functional electrodes: 3D graphene foam and ZnO nanocrystals, separator: glass fiber, and electrolyte: 1 M  $\text{LiPF}_6$  in EC/MC = 50/50. (b) The home-made capacitor mounting system.

**D. Methods:** Scanning electron microscopy (SEM) (JEOL, JSM-6010LV) and Raman spectroscopy (Renishaw inVia, excited by a 532 nm) were used to characterize the 3D graphene foam. The structure of the 3D foam-like graphene was verified by Raman data which were recorded at 532 nm laser source under  $2 \mu\text{m}$  spot size. The three-dimensional structure of graphene foam was analyzed by SEM imaging at 10 kV. X-band (9.86 GHz) EPR measurements were performed with Bruker EMX spectrometer using a rectangular TE102 (X-band) resonator. The magnetic field was determined using an NMR gaussmeter (ER 035M, Bruker); for the calibration of the magnetic-field measurement a polycrystalline DPPH with  $g = 2.0036$  was used. Cyclic voltammetry (CV), electrochemical galvanostatic cycling with potential limitation (GCPL) and electrical impedance spectroscopy (EIS) measurements were carried out using a VSP/VMP3 multichannel potentiostat/galvanostat (BioLogic) at room temperature. The CV tests were conducted at a scan rate of  $10 \text{ mV}\cdot\text{s}^{-1}$ . The GCPL tests were carried out at rate performance between 0.1 to 5 C. Electrochemical analysis in particular specific



capacity was calculated from GCPL data by the aid of EC-LAB V10.40 *BioLogic* software. EIS data were collected in the frequency range between 0.1 Hz and 100 kHz. For the analysis of the spectra we used ZView software. The amplitude of voltage modulation was set to 100 mV. A four-point electrode-setup was used to exclude the potential drop due to electrochemical reactions occurring at the working electrode(s). The setup consisted of steel screws as the current collector on which the electrode material was connected. Both electrodes were separated by a glass fiber and a 1 M LiPF<sub>6</sub> in EC/MC=50/50 were used as electrolyte.

### 3. Results and Discussion

Three sample Raman spectra taken at different points on the 3D-GF are shown in Fig 2. Graphene specific G and 2D peaks at 1590 cm<sup>-1</sup> and 2700 cm<sup>-1</sup>, respectively can be seen clearly in these spectra. The ratio of the signal intensities at 2D and G peaks confirm that 3D-GF has a varying thickness and in the sample traces single-, double-, and multi-layer graphene are identified. In addition, the absence of the D band around 1350 cm<sup>-1</sup>, an indication of defects and disordered carbon, signifies that the CVD-grown 3D-GF is of high quality<sup>43</sup>.

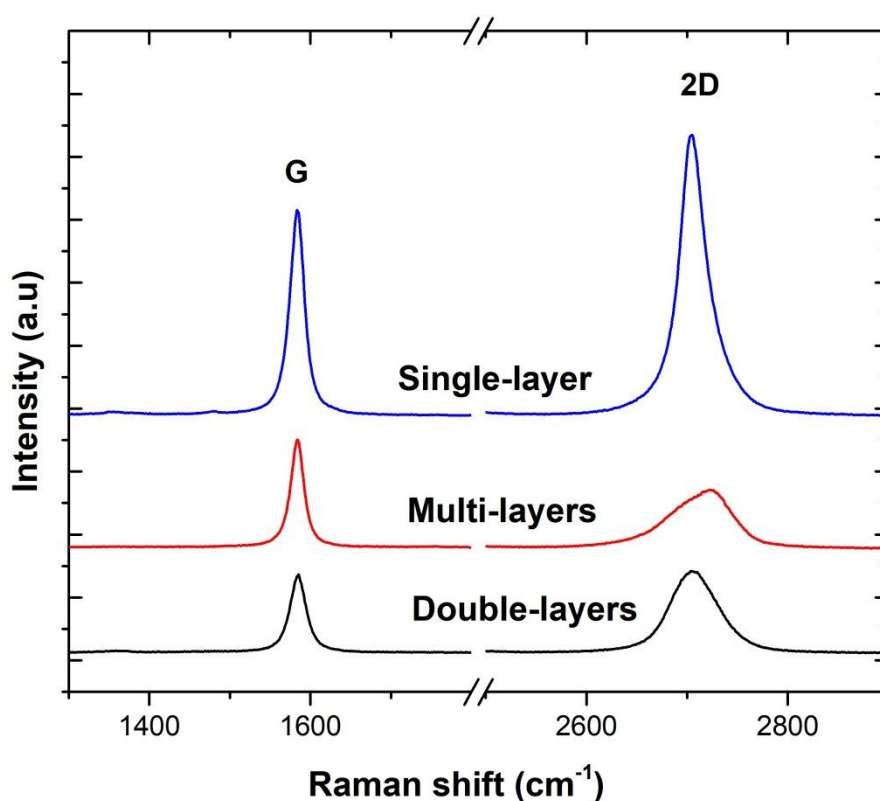


**Fig. 2:** Raman spectra of 3D-GF obtained at different positions.

Fig. 3(a) shows a photograph of the as-prepared GF which exhibits monolithic form with good mechanical stability and hence can easily be handled. Fig. 3(b and c) show SEM images of 3D-GF at different magnifications. As revealed by the photographs, a smooth graphene skeleton with a 3D structure is endured without any cracks validating interconnected network of the graphene foam.



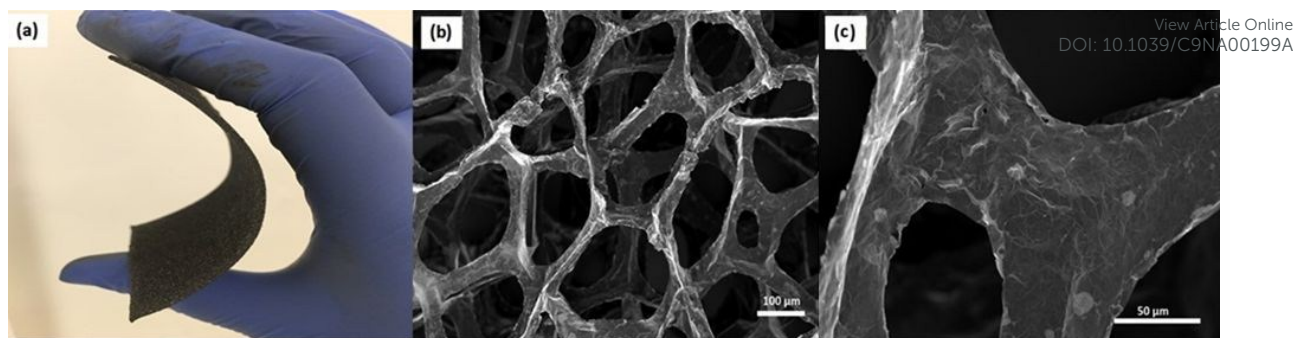


**Fig. 3:** (a) Photograph of 3D-GF, (b and c) SEM images of the 3D-GF with different magnifications.

Using multifrequency EPR (X- (9.86 GHz) and Q-band (35 GHz)) to detect and assign the defect kinds is a powerful approach. For this purpose ZnO and GF electrodes were investigated both X- and Q-band. The advantage of using multifrequency is attaining better sensitivity and ability of resolving anisotropy in  $g$ -factor and hyperfine structure if they exist. The ZnO electrode used here revealed two distinctive EPR spectra both in X- and Q-band which were reported and explained previously by Erdem *et al.* by the aid of so called core shell model<sup>11,17</sup>. According to this model, ZnO has paramagnetically active defect centers namely singly ionized  $V_O$ ,  $V_{Zn}$ , Zn and O interstitials. Assembly of such defects or defect complexes consisting of such paramagnetic active centers give two distinct EPR centers as shown in Fig. 4 (a) and (b), at  $g=1.962$  and  $g=2.006$  depending on their location inside the ZnO nanocrystal lattice. In case the ionized trapped electrons or holes are localized in the core/bulk sides of the crystal, they are more bound and feel larger spin-orbit coupling effect; causing a large deviation from the  $g \approx 2$  region and yielding a  $g$ -factor of 1.962. Whereas, if the ionized electrons are located near the surface they are delocalized and behave like free-electrons with  $g$ -factor of 2.006 ( $g_{\text{free-electron}}=2.0023$ ). These defect centers also contribute as conduction electrons and increase the conductivity of the ZnO sample enormously. Thus, nanoscale ZnO has different electrical transport properties than the bulk ZnO counterpart mainly due to the existence of defect centers. Such electrical transport properties of defects in ZnO nanocrystals have been presented earlier by the aid of EPR and two point dc electrical results<sup>11</sup>. We reported that the specific resistivity of ZnO is reduced drastically with decreasing the crystallite size, thus increasing the concentration of surface defects. Detailed EPR of systematically synthesized ZnO nanocrystals via solid state reaction method were already reported elsewhere<sup>13</sup> thus further analysis of EPR on ZnO sample here will be redundant.



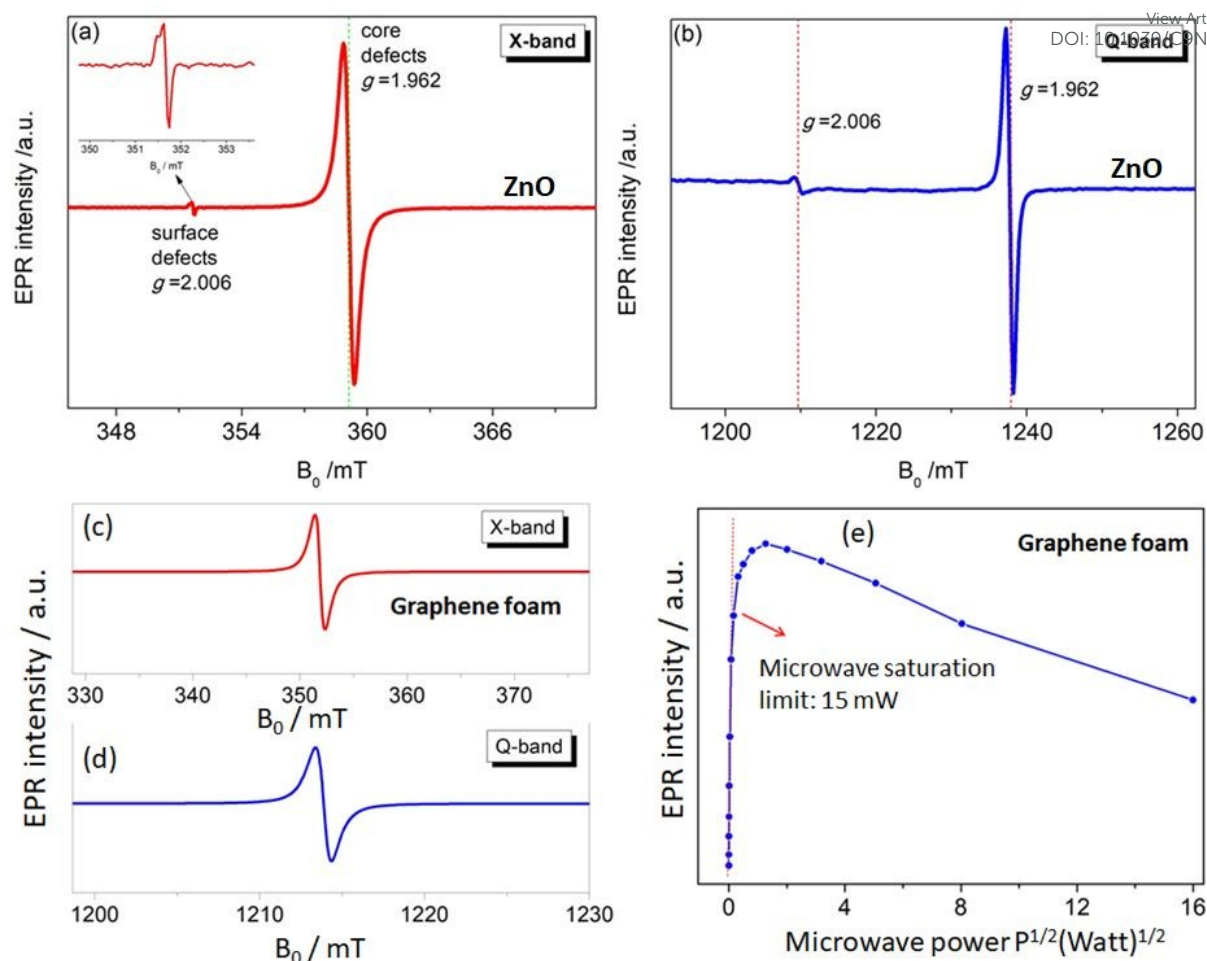


**Fig. 4:** Room temperature continuous wave EPR signals of ZnO nanocrystals measured at (a) X-band and (b) Q-band. Room temperature continuous wave EPR signals of GF measured at (c) X-band and (d) Q-band, respectively. (e) The EPR intensity extracted from the microwave power dependent spectra in order to understand the saturation behavior.

The defect structures of GO or rGO<sup>44</sup>, carbon nanotubes (CNT)<sup>45</sup>, carbon dots (Cdots)<sup>5</sup> has been investigated by EPR however there is no EPR report on 3D-GF. In Fig. 4 (c and d) X- and Q- band EPR of GF electrode is presented and Lorentzian line shape were obtained for both microwave frequency. Such single EPR spectra is expected for carbon related samples indicating defect centers due to dangling bonds and carbon radicals. Such defect centers can be correlated with the Raman data since disorder in graphene can be described by the intensity of D band. Although we did not observe any D-band in Raman spectra, nevertheless according to present EPR and Raman data defect contribution to conductivity is consistent and such crystallographic and electronic properties definitely play the key role for the performance of ultimate energy storage devices, here *superbats*. Of course we should admit that the conductivity discussion here is not done by a direct measurements but an indirect way via EPR and Raman. Anyway it is quite difficult task to understand the role of defects in GF and ZnO once both electrodes working synergistically together with electrolyte in the device. The correlation between Raman and EPR data has been further discussed below.

In order to understand in detail the dependency of the carbon related defects to the microwave power, we have investigated the saturation behavior of EPR spectra by X-band EPR. In Fig. 4 (e) the



peak-to-peak intensity of EPR spectra for GF signal rise with increasing microwave power. However, it deviates and starts damping strongly at 15 mW indicating saturation behavior. This observation represents that we can safely make EPR measurements below 15 mW without saturating the signal intensity. Furthermore, power saturation measurements in EPR spectroscopy give detailed information on the dynamic properties of defect centers. This procedure provides a simple alternative method to obtain spin-lattice ( $T_1$ ) or spin-spin ( $T_2$ ) relaxation data when direct-pulse-saturation EPR techniques are not available or are less suitable<sup>14,46</sup>. In EPR spectroscopy, it is well known that<sup>47</sup> easy-to-saturate systems have generally long relaxation times whereas hard-to-saturate systems have short relaxation times. From microwave power dependent measurements, it is seen that GF defect centers are highly steady due to its easy saturation behavior with inhomogeneous broadening of Gaussian line shape. In addition, the number of defect centers can be quantitatively determined by the aid of EPR spectra independent from the microwave frequency. In order to calculate the defect concentration, in other words the carbon concentration, one doubly integrates EPR first-derivative signal. By comparing the integral of the standard sample (here, MnO powder with  $1.495 \times 10^{18}$  spins) and the measured sample (here, GF) one gets the corresponding number of spins, thus the absolute concentration of defect center. For an accurate determination of defect concentration quantitatively, one has to carefully consider the spin counting procedure as indicated in a well-known text book<sup>48</sup> and in our previous publications<sup>11,14,15,41</sup>. According to the spin counting results,  $8.2 \times 10^{19}$  spins/g paramagnetic defects were obtained which is relatively high. Moreover,  $sp^2$ - and  $sp^3$ -hybridizations can be differentiated by their linewidths ( $\Delta B$ ) in the EPR spectra<sup>18,49–51</sup>. The linewidth for  $sp^3$ -hybridized carbon centers, as found in diamond for instance, has been determined as  $\Delta B_{sp^3} < 1$  mT, while for graphite-like carbon centers with  $sp^2$ -hybridization, generally a broader  $\Delta B_{sp^2} \geq 1$  mT is observed. The corresponding value of  $\Delta B$  for GF sample in X- and Q-band spectra presented in Fig. 4 (c and d) lie around 1.02 mT both in X- and Q- band spectra allowing us to experimentally determine the hybridization state of carbon. These results strongly support the mere presence of  $sp^2$ -bonding. Here one can extend the discussion to the absence of D-band and pronounced existence of two phonon 2D band in Raman results given in Fig. 2. It is well known that graphene has  $sp^2$  bonds between carbon atoms which are not related with the defect centers whereas  $sp^3$  bonds (like diamonds) are strongly related to the defect structures. Actually, the existence of structural defects in  $sp^2$ -hybridized carbon bonds reveals D-band in Raman spectra, and thus makes Raman spectroscopy one of the most sensitive methods to investigate defects in  $sp^2$  carbon materials, here GF. G-band in Fig. 2 is caused by scattering by Brillouin zone center phonons whereas the 2D-band (also referred to as  $G'$ ) has been observed when  $sp^2$  carbons exist and can be attributed to resonant Raman scattering processes<sup>52–54</sup>. The line shape and the relative intensity of the 2D-band can be used to determine the number and orientation of graphene layers in few layered graphene samples (1-5 layers)<sup>52</sup>. Indeed if the graphene is defect free 2D-band is expected to have high intensity and sharp in lineshape. Present Raman data highly suggest that the G- and 2D-bands are highly sensitive modes to the charge transfer induced in GF, which are due to the electron-phonon coupling induced renormalization of phonon energy. On the other hand, the absence of D-band suggests that the sample is defect free<sup>55,56</sup> while the D-band is caused by the disordered structure of in carbonaceous materials here 3D GF. However, the defects may not be visible in Raman spectra simply because of two main reasons. First, EPR active defect centers such as carbon dangling bonds and  $\pi$ -conjugated carbon radicals in GF has silent mode A2 which is Raman inactive. Second, their number is below the Raman detection limit if the measurement volume is small. This problem can be overcome by EPR technique, as its detection limit, approximately  $10^{11}$  spins<sup>57,58</sup>, is



extremely low compared to Raman spectroscopy. Moreover, Raman is somewhat an indirect observation of defect centers via phonon modes where the defect centers effect the Raman active vibrational modes but EPR is a direct method to detect the defect states. Thus, it is important to note that two methods have different detection mechanisms and sensitivity levels. Nevertheless, although Raman data does not indicate any defect structure (almost defect free) by the absence of D-band, both methods used here indicate  $sp^2$  bonding for the GF.

Finally, Fig. 5 (a, b, c, d) presents the outstanding electrochemical performance results of the *superbat* system produced from the electrode materials described above and characterized. Collectively, these results show that the assembled *superbat* performs close to perfection in its own frame. In Fig. 5(a) a typical pseudocapacitance CV profile is presented, meaning that the shape of CV relates to the energy storage mechanisms, i.e. rectangular for most EDLCs or quasi-rectangular for pseudocapacitors due to redox peaks<sup>59</sup>. It is well known that such Faradaic supercapacitors have surface confined I-V curves due to their kinetics. Their mechanism consists of two main parts: surface redox and intercalation process<sup>21</sup>. In both mechanism during the change in oxidation state and intercalation, unlike batteries, the oxidation state maintains its change continuously without any phase transition. Here, it shows highly reversible redox reactions and in addition presents very large extra charge capacities with a cathodic peak in the charging potential window from 0-1 V having maximum at 0.79 V and in the reverse process, an anodic peak in the discharging potential window from 0.12 V-1.5 V (negative) having minimum at -1.05 V. Such an extra charge capacity obtained by oxidation/reduction peak couples increase the system's conductivity as well as energy storage capacity. It is important to note that these peaks are of inherent existence of capacitive currents without any migrations or any kind of decomposition in electrodes or electrolyte materials. Such surface-related capacitive process increases the charge storage capabilities. Of course, it is not easy to distinguish here whether the high current peaks are due to redox active ZnO nanocrystal or 3D GF solely or both. Probably both electrodes including their defect structures on the surface have significant contributions simultaneously however they overlap at more or less the same range of voltage window and do not resolve here. That's why only one peak per redox is observable. Thus it is possible to conclude here that the extra charge storage at the interface of electrolyte and electrode materials, and efficient electron transport due to the increased number of surface defects affect the electrochemical behavior of *superbat*. Moreover, very large peak-to-peak potential separation and current peaks is a good observation of high electron transfer rate and a larger effective surface area for the *superbat* system. Of course we this statement is quite debating while a few scientists reported that large peak-to-peak potential separation is an indication of a poor performance due to a high resistance in the system due to low electron transfer rate. However, for instance such large shift in both cathodic and anodic peak has been attributed to edge-plane defects in graphite basal plane structures as electrode<sup>60,61</sup> resulting an extraordinary good electrochemical performance.



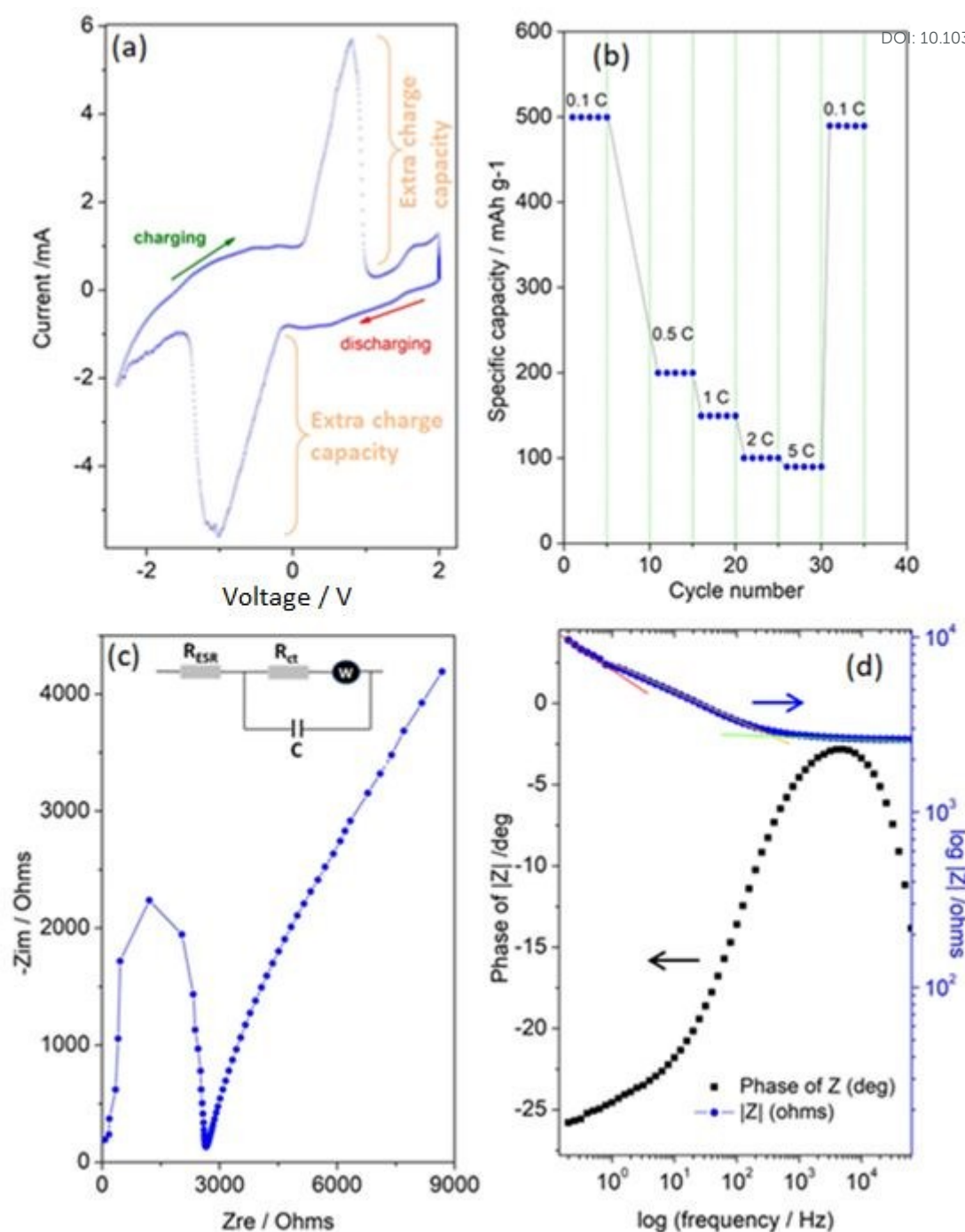


**Fig. 5:** Electrochemical performance results of the *superbat* designed with ZnO nanocrystal and graphene foam electrodes, LiPF<sub>6</sub> electrolyte and glass fiber separator. (a) Cyclic voltammetry (CV), (b) rate performance obtained from galvanostatic cycle with potential limitation (GCPL) technique. (c) Nyquist plot and (d) Bode plot obtained from electrochemical impedance spectroscopy (EIS).

In Fig. 5(b) rate performances were evaluated from 0.1 to 5 C with 5 cycles at each rate. Discharge capacities of 499, 199, 150, 99, and 89 mAhg<sup>-1</sup> are obtained at 0.1, 0.5, 1, 2 and 5 C, respectively. When tuning the current density back to 0.1 C, the capacity is mostly recovered having the value of 489 mAhg<sup>-1</sup>. Conventionally, this indicates good cycling stability of *superbat* at various current densities indicating a negligible loss of active material due to any dissolution or decomposition of electrolyte or electrodes or any kind of shuttling during cycling. The superior performance of the *superbat* can be ascribed to the GF's well-developed 3D porous structure and ZnO's nanoscale



particle size, hence defect structures. The high surface area micropores of GF can strongly adsorb extra conduction electrons due to defects, whereas the the distribution of defects on the surface of the small sized ZnO nanocrystals together facilitate rapid mass diffusion and transport to access the redox active sites. Therefore, when utilized as the *superbat* as a whole, electrodes can rapidly trap electrons due to defects and prevent their migration to enhance the *superbat* performance. At this point we have to emphasize that indeed ZnO is a battery-type material and not a pseudocapacitive one. The CV in Figure 5a is the typical of a battery, not a pseudocapacitive material which in normal conditions gives a rectangular shape CV. Actually, there is much confusion in the scientific literature between pseudocapacitance and battery capacity<sup>62,63</sup>. True pseudocapacitive materials are in general RuO<sub>x</sub> and MnO<sub>x</sub>, which provide typical rectangular CVs. If there are strong peaks as in this case, it is not pseudocapacitance behavior but battery behavior that's why we have named our system as *superbat* while this system both behave like battery and supercapacitor where capacity describes both the storage of energy and capacitance. Therefore one may say here that nano-sized ZnO shows exceptional extraordinary electrochemical performance behavior than the counterpart bulk ZnO due to its own surface defects<sup>14</sup>. More than this, two scenario can be put forward here for the significant electrochemical performance: i) due to lithium intercalation into the ZnO electrode lattice since many literature reported the Li-insertion into ZnO nanocrystals or ii) defect-assisted Li-intercalation into ZnO nanocrystals enhance the performance. One drawback here can be given as follows: from previous literature, the graphene 3D foam as supercapacitor electrode itself does not exhibit such redox-like cycling behaviors since it should be limited to surface adsorption processes during charging-discharging. Nyquist plot and Bode plot of phase angle and total impedance in Figs. 5(c) and (d) were obtained from the EIS data, respectively. EIS measurements can provide information on circuit components such as equivalent series resistors, capacitors, diffusion parameters and charge transfer resistances that cannot be obtained in more detail and clearly by CV or GCPL techniques. Fig. 5(c) shows a well-defined semi-circle showing a typical Nyquist property followed by a non-ohmic increase. In the inset of Fig. 5(c) equivalent Randless circuit of the system is given which is a common physical model of the electrode-electrolyte interface that is constructed according to the general rules described elsewhere<sup>64</sup>. According to this circuit, the system consists of the following electrical components: equivalent serial resistance ( $R_{ESR}$ ), an active charge transfer resistance ( $R_{ct}$ ), Warburg diffusion element ( $W$ ) and pseudocapacitance ( $C$ ). The EIS analyses revealed that the serial resistance of the *superbat* is 2.65 k $\Omega$  whereas charge transfer resistance  $R_{ct}$  is 8.65 k $\Omega$ . Here the existence of Warburg impedance element, indicating the readily diffusion of the electrolyte ions and good capacitive behavior as well<sup>65</sup>.  $R_{ct}$  and pseudocapacitance ( $C$ ) appear in Randless circuit due to surface roughness and conductivity difference between the electrodes and electrolyte. In Fig. 5(d) variation of the impedance as a function of the frequency confirms the corroboration of capacitance measurements while the curve follows the expected Kramers-Kronig relation which is an obvious increasing of the impedance at lower frequencies<sup>5,66</sup>. It shows three significant slopes at different frequency regions for the entire *superbat* system, in other words for the Randless circuit given in Fig. 5c inset. At the low-frequency region (0.1 Hz-0.7 Hz), the slope is quite steep (red line in Fig. 5(d)) which is due to the less conductive component of the interfaces. At the intermediate frequency region (0.7 Hz-700 Hz) the slope is somehow less (orange line in Fig. 5(d)) than the lower frequency range indicating both capacitive and resistive components of both electrodes at the interfaces are active and compete with each other. This more resistive region actually dominates the system by its wide range of frequency dependency. Finally, at high frequency region (>1000 Hz) the slope is almost flat (green line in Fig. 5(d)) meaning that *superbat* is highly capacitive at this range where capacitance  $C$  controls the overall system. Such frequency dependency



of impedance can be attributed to remarkable electrochemical performance of both electrodes giving a high specific capacitance and good rate capability in *superbat* system. The explanation for this is indeed quite simple: high conductivity of graphene foam assists as electron transfer pathway and enables easy transport of electrolyte ions ( $\text{PF}_6^-$ ,  $\text{Li}^+$ ) to the electrode surface. Moreover, the contact between surface defects in both electrodes and electrolyte is increased during the electrochemical reaction. Thus, defect structures play an important role in improving the electrochemical performance of *superbat* and prove that these electrode materials (ZnO and 3D GF) can be effectively used for the improvement of supercapacitors. The maximum point of Z-phase is also shown in Fig. 5d for  $-2.7^\circ$  (near  $0^\circ$ ) at 4.42 kHz which corresponds to the almost linear behavior (on the Bode plot of frequency versus impedance) with a slope of  $\sim 1$ . Finally, *superbat* exhibits the specific capacity of 498 mAh/g at 0.1 C and shows excellent rate capability. More importantly, pseudocapacitive *superbat* produced by the synergetic effects of ZnO and 3D GF electrodes can be operated in a two electrode system at 0-2 V voltage region and give a high specific capacitance of 448 F/g, which delivers a maximum energy density of 35 Wh/kg at a maximum power density of 270 W/kg.

#### 4. Conclusions

A special design *superbat* was constructed and the role of defect structures in ZnO and GF were investigated for the improvement of the electrochemical performance. Synergetic effects of both electrodes and the electrolyte revealed high values for energy density and power density. Here studied abovementioned electrode and electrolyte materials in depth and have found out that the intrinsic defect states play an essential role on the electrical and electronic properties which detailed investigations of such defects generally underestimated so far in the literature. Various state-of-art characterization techniques such as electron paramagnetic resonance, Raman and impedance spectroscopy have been undertaken in order to understand the origin of the performance of the hybrid capacitor in more depth. In particular, we obtained high capacitance value ( $C = 448 \text{ F/g}$ ) which is exceptionally related not only the quality of synthesis but also the choice of electrode and electrolyte materials. Moreover, not only each component used in the construction of the hybrid supercapacitor is playing a key role to achieve high capacitance value but also the smart design of supercapacitor design gives extensive control of mounting each component. This contribution contains interesting new science with different aspects of nanomaterials and defect-related science in such matter. It is therefore interesting for materials scientists, chemists as well as engineers working in the field of hybrid capacitors. Moreover, this work is of high interest to a variety of researchers working on the development of electrode materials for efficient supercapacitors.

#### Acknowledgements

This study was funded by The Scientific and Technological Research Council of Turkey (TUBITAK) under the grant No: 115Y344. The preparation and characterization of 3D-GF were conducted using equipment at Sabanci University SUNUM, Nanotechnology Research Center. E. Erdem thanks to Loire Valley General Programme for LE STUDIUM/Marie Skłodowska-Curie Research Fellowship and Dr. G. Poulin-Vittrant from University of Tours for fruitful discussion and support.



## References

View Article Online  
DOI: 10.1039/C9NA00199A

- 1 P. Simon and Y. Gogotsi, Capacitive energy storage in nanostructured carbon-electrolyte systems, *Accounts of chemical research*, 2013, **46**, 1094–1103.
- 2 M. Salanne, B. Rotenberg, K. Naoi, K. Kaneko, P.-L. Taberna, C. P. Grey, B. Dunn and P. Simon, Efficient storage mechanisms for building better supercapacitors, *Nature Energy*, 2016, **1**, 16070.
- 3 P. Simon, Y. Gogotsi and B. Dunn, Materials science. Where do batteries end and supercapacitors begin?, *Science (New York, N.Y.)*, 2014, **343**, 1210–1211.
- 4 S. Repp, E. Harputlu, S. Gurgen, M. Castellano, N. Kremer, N. Pompe, J. Wörner, A. Hoffmann, R. Thomann, F. M. Emen, S. Weber, K. Ocakoglu and E. Erdem, Synergetic effects of Fe<sup>3+</sup> doped spinel Li<sub>4</sub>Ti<sub>5</sub>O<sub>12</sub> nanoparticles on reduced graphene oxide for high surface electrode hybrid supercapacitors, *Nanoscale*, 2018, **10**, 1877–1884.
- 5 R. Genc, M. O. Alas, E. Harputlu, S. Repp, N. Kremer, M. Castellano, S. G. Colak, K. Ocakoglu and E. Erdem, High-Capacitance Hybrid Supercapacitor Based on Multi-Colored Fluorescent Carbon-Dots, *Scientific reports*, **7**, 11222.
- 6 M. Sawicki, A. L. Ortiz, M. Luo and L. L. Shaw, Structural-Defect-Controlled Electrochemical Performance of Sodium Ion Batteries with NaCrO<sub>2</sub> Cathodes, *ChemElectroChem*, 2017, **4**, 3222–3230.
- 7 P. Gao, P. Metz, T. Hey, Y. Gong, D. Liu, D. D. Edwards, J. Y. Howe, R. Huang and S. T. Mixture, The critical role of point defects in improving the specific capacitance of δ-MnO<sub>2</sub> nanosheets, *Nature Communications*, 2017, **8**, 14559.
- 8 M. Y. HO, P. S. KHIEW, D. ISA, T. K. TAN, W. S. CHIU and C. H. CHIA, A review of metal oxide composite electrode materials for electrochemical capacitors, *NANO*, 2014, **09**, 1430002.
- 9 T. Kou, B. Yao, T. Liu and Y. Li, Recent advances in chemical methods for activating carbon and metal oxide based electrodes for supercapacitors, *J. Mater. Chem. A*, 2017, **5**, 17151–17173.
- 10 Y. Wang, X. Xiao, H. Xue and H. Pang, Zinc Oxide Based Composite Materials for Advanced Supercapacitors, *ChemistrySelect*, 2018, **3**, 550–565.
- 11 S. K. S. Parashar, B. S. Murty, S. Repp, S. Weber and E. Erdem, Investigation of intrinsic defects in core-shell structured ZnO nanocrystals, *J. Appl. Phys.*, 2012, **111**, 113712.
- 12 S. Repp, S. Weber and E. Erdem, Defect Evolution of Nonstoichiometric ZnO Quantum Dots, *J. Phys. Chem. C*, 2016, **120**, 25124–25130.
- 13 S. Repp and E. Erdem, Controlling the exciton energy of zinc oxide (ZnO) quantum dots by changing the confinement conditions, *Spectrochimica acta. Part A, Molecular and biomolecular spectroscopy*, 2016, **152**, 637–644.
- 14 E. Erdem, Microwave power, temperature, atmospheric and light dependence of intrinsic defects in ZnO nanoparticles, *Journal of Alloys and Compounds*, 2014, **605**, 34–44.
- 15 J. J. Schneider, R. C. Hoffmann, J. Engstler, A. Klyszcz, E. Erdem, P. Jakes, R.-A. Eichel, L. Pitta-Bauermann and J. Bill, Synthesis, Characterization, Defect Chemistry, and FET Properties of Microwave-Derived Nanoscaled Zinc Oxide, *Chem. Mater.*, 2010, **22**, 2203–2212.
- 16 P. Jakes and E. Erdem, Finite size effects in ZnO nanoparticles, *Phys. Status Solidi RRL*, 2011, **5**, 56–58.
- 17 H. Kaftelen, K. Ocakoglu, R. Thomann, S. Tu, S. Weber and E. Erdem, EPR and photoluminescence spectroscopy studies on the defect structure of ZnO nanocrystals, *Phys. Rev. B*, 2012, **86**, 14113.
- 18 A. Bateni, E. Erdem, S. Repp, S. Acar, I. Kokal, W. Häßler, S. Weber and M. Somer, Electron paramagnetic resonance and Raman spectroscopy studies on carbon-doped MgB<sub>2</sub> superconductor nanomaterials, *Journal of Applied Physics*, 2015, **117**, 153905.



- 19 C. van Pham, S. Repp, R. Thomann, S. Weber, M. Krueger and E. Erdem, Charge transfer and surface defect healing within ZnO nanoparticle decorated graphene hybrid materials, *Nanoscale*, 2016.
- 20 W.-Y. Tsai, R. Lin, S. Murali, L. Li Zhang, J. K. McDonough, R. S. Ruoff, P.-L. Taberna, Y. Gogotsi and P. Simon, Outstanding performance of activated graphene based supercapacitors in ionic liquid electrolyte from  $-50$  to  $80^{\circ}\text{C}$ , *Nano Energy*, 2013, **2**, 403–411.
- 21 X. Yu, S. Yun, J. S. Yeon, P. Bhattacharya, L. Wang, S. W. Lee, X. Hu and H. S. Park, Emergent Pseudocapacitance of 2D Nanomaterials, *Adv. Energy Mater.*, 2018, **8**, 1702930.
- 22 Z. Chen, W. Ren, L. Gao, B. Liu, S. Pei and H.-M. Cheng, Three-dimensional flexible and conductive interconnected graphene networks grown by chemical vapour deposition, *Nature materials*, 2011, **10**, 424.
- 23 Q. Fang, Y. Shen and B. Chen, Synthesis, decoration and properties of three-dimensional graphene-based macrostructures, *Chemical Engineering Journal*, 2015, **264**, 753–771.
- 24 H.-P. Cong, J.-F. Chen and S.-H. Yu, Graphene-based macroscopic assemblies and architectures, *Chemical Society reviews*, 2014, **43**, 7295–7325.
- 25 L. Zhang and G. Shi, Preparation of Highly Conductive Graphene Hydrogels for Fabricating Supercapacitors with High Rate Capability, *J. Phys. Chem. C*, 2011, **115**, 17206–17212.
- 26 Y.-C. Yong, X.-C. Dong, M. B. Chan-Park, H. Song and P. Chen, Macroporous and monolithic anode based on polyaniline hybridized three-dimensional graphene for high-performance microbial fuel cells, *ACS nano*, 2012, **6**, 2394–2400.
- 27 M. T. Pettes, H. Ji, R. S. Ruoff and L. Shi, Thermal transport in three-dimensional foam architectures of few-layer graphene and ultrathin graphite, *Nano Letters*, 2012, **12**, 2959–2964.
- 28 H. Lin, S. Xu, X. Wang and N. Mei, Significantly reduced thermal diffusivity of free-standing two-layer graphene in graphene foam, *Nanotechnology*, 2013, **24**, 415706.
- 29 D. R. Dreyer, S. Park, C. W. Bielawski and R. S. Ruoff, The chemistry of graphene oxide, *Chemical Society reviews*, 2010, **39**, 228–240.
- 30 S. Park and R. S. Ruoff, Chemical methods for the production of graphenes, *Nature nanotechnology*, 2009, **4**, 217–224.
- 31 D. Li, M. B. Müller, S. Gilje, R. B. Kaner and G. G. Wallace, Processable aqueous dispersions of graphene nanosheets, *Nature nanotechnology*, 2008, **3**, 101.
- 32 S. Nardecchia, D. Carriazo, M. L. Ferrer, M. C. Gutiérrez and F. del Monte, Three dimensional macroporous architectures and aerogels built of carbon nanotubes and/or graphene, *Chemical Society reviews*, 2013, **42**, 794–830.
- 33 C. Li and G. Shi, Three-dimensional graphene architectures, *Nanoscale*, 2012, **4**, 5549–5563.
- 34 J. Zhu, A. S. Childress, M. Karakaya, S. Dandeliya, A. Srivastava, Y. Lin, A. M. Rao and R. Podila, Defect-Engineered Graphene for High-Energy- and High-Power-Density Supercapacitor Devices, *Advanced materials (Deerfield Beach, Fla.)*, 2016, **28**, 7185–7192.
- 35 V. Sridhar, H.-J. Kim, J.-H. Jung, C. Lee, S. Park and I.-K. Oh, Defect-engineered three-dimensional graphene-nanotube-palladium nanostructures with ultrahigh capacitance, *ACS Nano*, 2012, **6**, 10562–10570.
- 36 G. Li, G. R. Blake and T. T. M. Palstra, Vacancies in functional materials for clean energy storage and harvesting, *Chemical Society reviews*, 2017, **46**, 1693–1706.
- 37 A. G. Pandolfo and A. F. Hollenkamp, Carbon properties and their role in supercapacitors, *Journal of Power Sources*, 2006, **157**, 11–27.
- 38 W. Zuo, R. Li, C. Zhou, Y. Li, J. Xia and J. Liu, Battery-Supercapacitor Hybrid Devices, *Advanced science (Weinheim, Baden-Wuerttemberg, Germany)*, 2017, **4**, 1600539.



- 39 E. Frackowiak, Q. Abbas and F. Béguin, Carbon/carbon supercapacitors, *Journal of Energy Chemistry*, 2013, **22**, 226–240. High Article Online  
DOI: 10.1039/C9NA00199A
- 40 T. Chen and L. Dai, Carbon nanomaterials for high-performance supercapacitors, *Materials Today*, 2013, **16**, 272–280.
- 41 A. Bateni, E. Erdem, S. Repp, S. Weber and M. Somer, Al-doped MgB<sub>2</sub> materials studied using electron paramagnetic resonance and Raman spectroscopy, *Appl. Phys. Lett.*, 2016, **108**, 202601.
- 42 S. K.S. Parashar, B. S. M., S. Repp, S. Weber and E. Erdem, Investigation of intrinsic defects in core-shell structured ZnO nanocrystals, *Journal of Applied Physics*, 2012, **111**, 113712.
- 43 K. S. Novoselov, D. Jiang, F. Schedin, T. J. Booth, V. V. Khotkevich, S. V. Morozov and A. K. Geim, Two-dimensional atomic crystals, *Proceedings of the National Academy of Sciences of the United States of America*, 2005, **102**, 10451–10453.
- 44 D. Savchenko and A. H. Kassiba, *Frontiers in Magnetic Resonance*, BENTHAM SCIENCE PUBLISHERS, 2018.
- 45 C. V. Pham, M. Krueger, M. Eck, S. Weber and E. Erdem, Comparative electron paramagnetic resonance investigation of reduced graphene oxide and carbon nanotubes with different chemical functionalities for quantum dot attachment, *Appl. Phys. Lett.*, 2014, **104**, 132102.
- 46 A. Lund, E. Sagstuen, A. Sanderud and J. Maruani, Relaxation-time determination from continuous-microwave saturation of EPR spectra, *Radiation research*, 2009, **172**, 753–760.
- 47 John A. Weil and James R. Bolton, *Electron Paramagnetic Resonance 2e*.
- 48 G. R. Eaton, S. S. Eaton, D. P. Barr and R. T. Weber, *Quantitative EPR. A Practitioners Guide*, Springer Verlag Wien, s.l., 1st edn., 2010.
- 49 E. Erdem, V. Mass, A. Gembus, A. Schulz, V. Liebau-Kunzmann, C. Fasel, R. Riedel and R.-A. Eichel, Defect structure in lithium-doped polymer-derived SiCN ceramics characterized by Raman and electron paramagnetic resonance spectroscopy, *Phys. Chem. Chem. Phys.*, 2009, **11**, 5628.
- 50 B. L. V. Prasad, H. Sato, T. Enoki, Y. Hishiyama, Y. Kaburagi, A. M. Rao, P. C. Eklund, K. Oshida and M. Endo, Heat-treatment effect on the nanosized graphite  $\pi$ -electron system during diamond to graphite conversion, *Phys. Rev. B*, 2000, **62**, 11209–11218.
- 51 O. Chauvet, L. Zuppiroli and I. Solomon, Electronic properties of disordered SiC materials, *Materials Science and Engineering: B*, 1992, **11**, 303–306.
- 52 C. Sole, N. E. Drewett and L. J. Hardwick, In situ Raman study of lithium-ion intercalation into microcrystalline graphite, *Faraday discussions*, 2014, **172**, 223–237.
- 53 V. N. Popov, Two-phonon Raman bands of bilayer graphene, *Carbon*, 2015, **91**, 436–444.
- 54 Y. Stubrov, A. Nikolenko, V. Gubanov and V. Strelchuk, Manifestation of Structure of Electron Bands in Double-Resonant Raman Spectra of Single-Walled Carbon Nanotubes, *Nanoscale research letters*, 2016, **11**, 2.
- 55 M. Kole and T. K. Dey, Investigation of thermal conductivity, viscosity, and electrical conductivity of graphene based nanofluids, *J. Appl. Phys.*, 2013, **113**, 84307.
- 56 A. C. Ferrari and D. M. Basko, Raman spectroscopy as a versatile tool for studying the properties of graphene, *Nature nanotechnology*, 2013, **8**, 235–246.
- 57 G. Feher, Sensitivity Considerations in Microwave Paramagnetic Resonance Absorption Techniques, *Bell System Technical Journal*, 1957, **36**, 449–484.
- 58 L. Zhang, E. Erdem, X. Ren and R.-A. Eichel, Reorientation of (MnTi<sup>IV</sup>-VO<sup>••</sup>)<sub>x</sub> defect dipoles in acceptor-modified BaTiO<sub>3</sub> single crystals, *Appl. Phys. Lett.*, 2008, **93**, 202901.
- 59 M. Moussa, M. F. El-Kady, Z. Zhao, P. Majewski and J. Ma, Recent progress and performance evaluation for polyaniline/graphene nanocomposites as supercapacitor electrodes, *Nanotechnology*, 2016, **27**, 442001.



- 60 J. Li, A. Cassell, L. Delzeit, J. Han and M. Meeyappan, Novel Three-Dimensional Electrodes, *J. Phys. Chem. B*, 2002, **106**, 9299–9305. Article Online  
DOI: 10.1039/C9NA00199A
- 61 J. Yang and S. Gunasekaran, Electrochemically reduced graphene oxide sheets for use in high performance supercapacitors, *Carbon*, 2013, **51**, 36–44.
- 62 T. Brousse, D. Belanger and J. W. Long, To Be or Not To Be Pseudocapacitive?, *Journal of the Electrochemical Society*, 2015, **162**, A5185-A5189.
- 63 S. Roldán, D. Barreda, M. Granda, R. Menéndez, R. Santamaría and C. Blanco, An approach to classification and capacitance expressions in electrochemical capacitors technology, *Physical chemistry chemical physics : PCCP*, 2015, **17**, 1084–1092.
- 64 A. S. Bandarenka, Exploring the interfaces between metal electrodes and aqueous electrolytes with electrochemical impedance spectroscopy, *The Analyst*, 2013, **138**, 5540–5554.
- 65 D. Sun, X. Yan, J. Lang and Q. Xue, High performance supercapacitor electrode based on graphene paper via flame-induced reduction of graphene oxide paper, *Journal of Power Sources*, 2013, **222**, 52–58.
- 66 J. M. Esteban, On the Application of the Kramers-Kronig Relations to Evaluate the Consistency of Electrochemical Impedance Data, *J. Electrochem. Soc.*, 1991, **138**, 67.

